Mohamed Boudiaf KOURA[1], Ahmed Hamida BOUDINAR[1], Azeddine BENDIABDELLAH[1], Ameur Fethi AIMER[1], Zakaria GHERABI[1]

Laboratory of Electric Drives Development, Diagnosis Group, Department of Electrical Engineering, University of Sciences and Technology of Oran, Oran, Algeria (1)

doi:10.15199/48.2021.03.24

Rotor Faults Diagnosis by Adjustable Window Function

Abstract. *Several recent studies dealing with new diagnosis methods criticize the classical method of Power Spectral Density by periodogram technique for its drawbacks related to frequency resolution. This is reflected by the appearance of a smoothing and a negative effect following the selected window function. Indeed, this technique is less efficient in the detection of frequency signatures of faults close to a high amplitude harmonic. In addition, it is unable to detect an incipient fault. However, this method has several advantages such as a low computation time and easy programming. To avoid these drawbacks while considering the method advantages, this paper proposes a simple procedure to define precisely the shape parameters of a new window belonging to the raised-cosine family. This procedure uses the characteristics of the stator current spectrum to ensure reliable diagnosis in the case of an incipient fault, while maintaining a quick processing time. The experimental tests carried out prove the effectiveness of the suggested approach in the diagnosis of incipient fault affecting an induction motor.*

Streszczenie. *Kilka ostatnich badań dotyczących nowych metod diagnostycznych krytykuje klasyczną metodę gęstości widmowej mocy techniką periodogramu ze względu na jej wady związane z rozdzielczością częstotliwości. Rzeczywiście, ta technika jest mniej skuteczna w wykrywaniu sygnatur częstotliwości uszkodzeń blisko harmonicznej o dużejj amplitudzie. Ponadto nie jest w stanie wykryć początkowej usterki. Jednak ta metoda ma kilka zalet, takich jak krótki czas obliczeń i łatwe programowanie. Aby uniknąć tych wad, biorąc pod uwagę zalety metody, w niniejszym artykule zaproponowano prostą procedurę precyzyjnego zdefiniowania parametrów kształtu nowego okna należącego do rodziny podniesionych cosinusów. Ta procedura wykorzystuje właściwości widma prądu stojana, aby zapewnić niezawodną diagnozę w przypadku początkowej fazy uszkodzenia, przy jednoczesnym zachowaniu szybkiego czasu przetwarzania. Przeprowadzone testy eksperymentalne dowodzą skuteczności sugerowanego podejścia w diagnozowaniu początkowej fazy uszkodzenia występującej w silnik indukcyjny (**Diagnostyka uszkodzeń wirnika z wykorzystaniem regulowanej funkcji okna**).*

Keywords: Diagnostic, Induction Motor, Rotor fault, Spectral analysis, Window Shape parameter
Słowa kluczowe: Diagnostyka, Silnik indukcyjny, Usterka wirnika, Analiza spektralna, Parametr kształtu Okno

Introduction

Induction motors are widely used in many industrial applications due to their low cost and high robustness. However, some failures can affect these motors; there are classified in three categories: faults related to the stator; rotor faults and mechanical faults. Furthermore, rotor faults represent 10 % of total induction motor failures. But now, they represent approximately 7 % of total failures, while stator faults remain around 21% [1]–[3], this change is due to the improvement in design and manufacture of cage rotors.

Rotor faults occur when one or more bars are broken. In this case, the current is no more flowing through these broken bars. This fault is generally caused by various constraints such as [3]–[5] thermal, magnetic, mechanical, residual or environmental constraints. The broken bar usually appears at the junction point between the short-circuit ring and the bars. This fault does not cause motor shutdown, but it can lead to reduced starting performance, load torque fluctuations or an increase of motor temperature [6]. This will obviously lead to motor degradation and will reduce its lifetime, if it is not detected in time. It is therefore logical, from an industrial, scientific and financial point of view, to diagnose this type of fault from its first stage.

Among all the diagnosis techniques of this fault [1], [7], [8], [9], [10]. It must be noticed that stator current analysis (or MCSA Motor Current Signature Analysis) is the technique that has been used more and more in recent years [11], [12]. This interest is due to its main advantage, namely easy installation of the sensor without disturbing the motor's operation. In addition, the current spectrum obtained presents a wealth of information on almost all the faults which can affect the induction motor [12]–[14].

Several studies [5], [12], [15], [16] using this technique, show that the rotor fault appears as a frequency signature around the fundamental. To identify this signature in industry, the Power Spectral Density (PSD) estimation is widely used because it has a simple programming and a fast execution, which is the main advantage of this method.

However, this approach cannot detect the signatures of the faults when they are very near to a high amplitude harmonic. A second drawback of this method is the impact of side lobes depending on the chosen window like Blackman, Hamming or Hanning. This second drawback does not allow the incipient faults to be detected [12].

In order to avoid these problems, several high-resolution spectral methods have been developed to analyze this kind of fault [1], [13], [17], [18]. These methods such as PRONY [13], MUSIC [1], or ESPRIT[17], [18], have an excellent frequency resolution even if the signal acquisition time is very short.

However, these methods have a major drawback; the computation time, which is relatively important due to the complexity of their algorithms.

To solve this problem, several researchers prefer to use the classic method of PSD for its main advantage, the computation time, by improving the windows function. To this end, several windows have been proposed in literature: the Papoulis window [19], the optimized trapezoidal window [20], the modified version of the classic Hamming window [21] and the Kaiser window [12]. These windows offer a better compromise between a narrow main lobe and low amplitude side lobes, which improves the detection of incipient faults using the PSD method.

For this reason, a new window belonging to the raised-cosine family is suggested in this work to improve the PSD estimation. This window has two parameters that can be adjusted as needed: the window's length and a variable parameter used to control the spectral characteristics of the window. In addition, a mathematical relationship is proposed to determine, the shape parameters appropriately which allow to obtain a reliable diagnosis in the case of an incipient fault. To show the efficacy of the proposed window on the diagnosis quality, several experimental tests have been carried out. The results obtained prove the advantages of the proposed approach.

Frequency Signatures of a Rotor Fault

The rotor faults are illustrated by two frequency signatures [22]–[24]:

- The first signature as lateral components f_{bb} around the fundamental as shown in Fig.1.

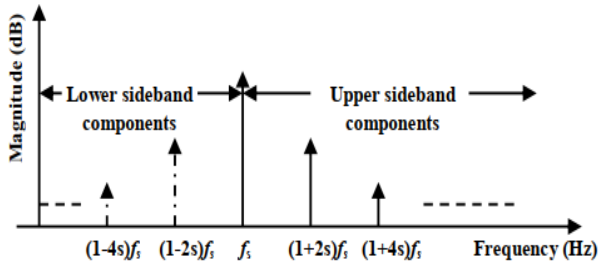

Fig.1. Rotor fault signature frequency around the fundamental.

The magnitudes of these components are proportional to the number of broken bars and to the motor load. This signature is expressed by the following equation:

$$f_{bb} = f_s(1 \pm 2ks). \qquad k = 1,2,3,... \tag{1}$$

where f_s is the power supply frequency, f_{bb} the rotor fault signatures and s the slip. In this paper, this frequency signature is analyzed.

The second signature is located around the space harmonics. This signature also considered as a decisive indicator to diagnose this type of faults [14]. It can be expressed by this relationship [25], [26].

$$f_{bb} = \left[\frac{k}{p}(1-s) \pm v\right] f_s \tag{2}$$

where p is the number of pole pairs, v = ± 1, ± 3, ± 5 is the order of the time harmonics of the Magneto-Motive Force and k/p = 1, 3, 5.

Estimation of The PSD by Periodogram Technique

PSD estimation is used when the signal to be analyzed is acquired in the steady state. This method is a frequency analysis approach applied to random signals of stationary types. In these cases, the PSD of the digitized current $i(n)$ may be described as follows [1], [27]:

$$PSD(k.\Delta f) = \frac{1}{N}\left|I(k.\Delta f)\right|^2 \tag{3}$$

where N is the samples number, $I(k.\Delta f)$ the Discrete Fourier Transform (DFT) of the measured stator current $i(n)$ and Δf the frequency resolution:

$$\Delta f = \frac{F_{sp}}{N} = \frac{1}{T_{acq}} \tag{4}$$

F_{sp} and T_{acq} are respectively the sampling frequency and the acquisition time.

It should be noted that the signal to be analyzed is limited in time due to its digitization. This is equivalent to performing the following mathematical operation:

$$i_T(n) = i(n).\Pi(n) \text{ with } n = 0,1,2,\ldots \text{ N-1} \tag{5}$$

Where $i_T(n)$ is the truncated digitized signal of $i(n)$, $\Pi(n)$ is a rectangular function of length N which represents the effect of the time limitation. In the frequency domain (5) is written as:

$$I_T(k.\Delta f) = I(k.\Delta f) \otimes N.Sinc(Nk.\Delta f) \tag{6}$$

$I_T(k.\Delta f)$ and $Sinc(Nk.\Delta f)$ are respectively the DFT of $i_T(n)$ and $\Pi(n)$, the operator ⊗ represents the convolution operation.

Equation (6) reveals that this truncation operation causes undesirable effects in the spectrum estimation, namely:

- An impossible localization of harmonics closes to each other in the case of signals processed over short acquisition times.
- An inability to identify low amplitude harmonics when side lobes appear due to $Sinc(Nk.\Delta f)$. Reducing the finesse of the analysis, which affects the detection of incipient faults.

To reduce these negative effects, the concept of windows is introduced. This means that instead of processing the truncated signal $i_T(n)$, we process the weighted signal given by this equation:

$$i_W(n) = i_T(n).\omega(n) \tag{7}$$

where $i_w(n)$ is the weighted current using the window function $\omega(n)$.

A window is defined by a given mathematical function which the principal parameters are:

- The main lobe width (L) at mid-height (at -3dB).
- The maximum magnitude of the side lobes (A).

These parameters are illustrated in Fig. 2.

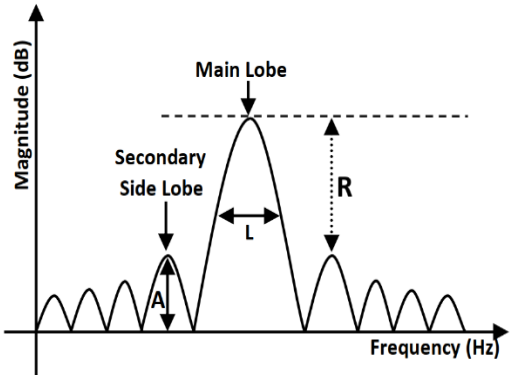

Fig.2. Representation a function window parameters.

R represents the ratio between the amplitude of the main lobe and the maximum amplitude of the side lobes expressed in dB. This parameter R indicates the interaction between the spectral lines [12].

A right choice of the window $\omega(n)$ allows:

- The reduction of the main lobes, thus enabling the harmonics identification close to each other.
- The attenuation of the side lobes magnitudes, thus enabling the detection of incipient defects.

Sadly, it is impossible to obtain these two characteristics at the same time, what affects the diagnosis reliability.

To solve these problems, several windows are used. In this work, a new solution belonging to the Raised-cosine family window is proposed for the flexibility of this family.

Raised-Cosine's Windows Family

K. M. M. Prabhu developed the Raised-cosine family. This window $w_{RC}(t)$ was synthesized from the Hanning and Rectangular windows. $w_{RC}(t)$ is defined as shown in the following equation [28]–[30]:

$$w_{RC}(t) = \begin{cases} \dfrac{1-2D}{2}\left(1+\cos\left(\dfrac{\pi t}{\tau}\right)\right) + 2D\left(\cos\left(\dfrac{2\pi t}{\tau}\right)\right), & |t| \le \tau \\ 0 & \text{elsewhere} \end{cases} \tag{8}$$

were τ represents the duration of the window and *D* is a constant shape parameter.

The best-known forms of this family according to references [29], [30], are where *D* = 0.0113, 0.0138, 0.0155 and 0.0165. Note that the magnitude of the side lobes varies between -42 dB and -51 dB but the width of the main lobe (–3dB) remains almost constant at 1.43Δf, with a Rate of Fall for off-Side-Lobe Level (RFSLL) equal to -6 dB/Octave for these values of *D*. The Hanning window is a special case of the raised-cosine family with *D* = 0.

A New Adjustable Window Developed

Several windows are proposed [29] in the form of sums, products, divisions or convolutions of simple trigonometric functions or deduced from other windows. This is the reason why in this paper, a new window function $w_R(t)$ based on the raised-cosine family is proposed. The purpose of this modification is to find an adjustable window that makes it easier to explore the compromise between the width of the main lobe and the amplitude of the side lobes related to the chosen window, which improves the detection of incipient faults. The various modifications made to the general shape of the Raised-cosine family to improve its performance are:

1st step: Replacement of the term cosine by a sine.

This change in trigonometric form aims to improve RFSLL of the raised-cosine family. The idea of this modification is inspired by the Papoulis window, given its characteristics for a better RFSLL -24 (dB / octave) and a ratio of the energy of the main lobe compared to the total energy higher than that of conventional windows such as Hanning, Hamming and Kaiser [28], [30]. The Papoulis window is nothing other than a summation of two trigonometric functions, a sine and a cosine. This change is indicated in the following equation:

$$(9)\quad w_R(t)=\begin{cases}\dfrac{1-2D}{2}\left(1+\sin\left(\dfrac{\pi t}{\tau}\right)\right)+2D\left(\cos\left(\dfrac{2\pi t}{\tau}\right)\right), & |t|\le\tau\\ 0 & \text{elsewhere}\end{cases}$$

2nd step: Determination of the shape parameter *D*.

The purpose of this step is to normalize the proposed window in order to ensure that the bell of its temporal form is similar to that of the normalized form of conventional windows. In other words, ensure that the start and end of the proposed window are equal to zero, which makes it possible to reduce the spectral leaks and to improve estimation of the amplitude in the frequency domain. For this reason, the value of parameter *D* will be calculated by solving equation (9) when t = 0. In this case, *D* equal to-1/2.

3rd step: Division of $w_R(t)$ by a constant equal to 3.

Equation (9) will be divided into 3 by considering the value of *D* obtained in 2nd step. The aim of this division is to reduce the effect of the continuous component of the function $w_R(t)$ on the analyzed spectrum. The following figure shows the time window of the proposed window after the modifications.

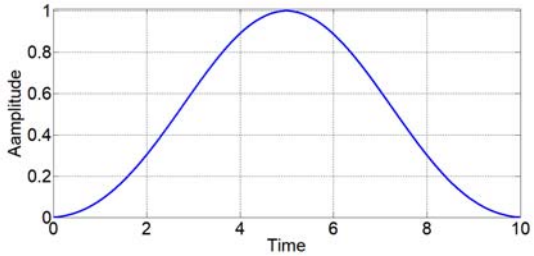

Fig.3. The temporal form of the proposed window for *D* = -1/2.

4th step: Introduction of a new *Z* shape parameter.

To provide a better flexibility compared to the raised-cosine family, a new *Z* parameter is proposed.

$$(10)\quad w_R(t)=\begin{cases}\left[\dfrac{1-2D}{6}\left(1+\sin\left(\dfrac{\pi t}{\tau}\right)\right)+\dfrac{2D}{3}\cos\left(\dfrac{2\pi t}{\tau}\right)\right]^Z, & |t|\le\tau\\ 0 & \text{elsewhere}\end{cases}$$

Z: is a positive real number.

It should be noted that a judicious choice of *Z* would allow us to find certain known windows. For example, for *Z* = 0, it is like the spectrum of the Rectangular window. In addition, when *Z* = 1.1, it is similar to the Hanning window and for *Z* = 2.6, this window is similar to the Blackman window.

Calculation of The Z Parameter

In this case, the discussion focuses on the choice of the *Z* parameter, which is decisive in the design of the window, because it determines the compromise between a narrow main lobe and secondary lobes of low magnitudes. Therefore, this choice is very important to improve the fault diagnosis in induction motors.

According to several tests carried out for different values of *Z*, the variation of this parameter has a direct influence on the variation of the ratio *R* as shown in this figure:

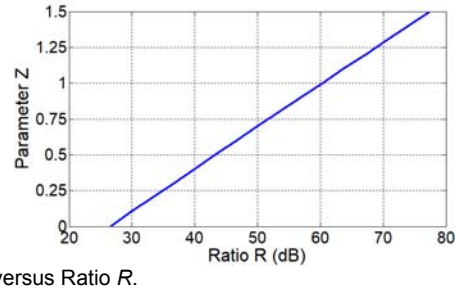

Fig.4. *Z* versus Ratio *R*.

From this figure, it is noticeable that the relation between the ratio *R* and the *Z* shape parameter of the proposed window is an almost linear function. This relationship can therefore be expressed mathematically in (11):

$$(11)\qquad Z\approx\frac{3R-80}{100},\qquad Z\ge 0$$

NB: This mathematical relationship is determined according to the characteristics of the motor used in this paper (see Appendix). The mathematical relation (11) shows that a simple determination of the ratio *R* from the spectrum of the current makes it possible to make an optimal calculation of the variable *Z*.

The following table presents a comparative study between the frequency characteristics of the proposed window for two different values of *Z* with the most used windows [30].

Table 1. Characteristics of the Windows function.

Windows	Side Lobe Level	Main Lobe Width (at -3 dB)
Rectangular	-13 dB	0.89 Δf
Hanning	-31.4 dB	1.44 Δf
Hamming	-42.8 dB	1.33 Δf
Proposed window (*Z*=1)	-31 dB	1.28 Δf
Proposed window (*Z* =2.5)	-56 dB	1.75 Δf

From Table 1, it can be seen that increasing the parameter Z makes it possible to obtain a better attenuation of the maximum level of the side lobes compared to other conventional windows (Hanning, Hamming, Rectangular).

This attenuation will allow us to extract the frequency signatures of a low amplitude as for the case of incipient faults, but unfortunately this attenuation is accompanied by an increase in the width of the main lobe (at -3dB), which reduces the frequency resolution and makes it impossible to extract signatures close to each other.

Thus, it is clear that the proposed window has the advantage of being a window with variable parameters recommended for the detection of incipient faults.

In addition, to confirm the positive contribution of this solution with respect to the computation time, several simulation tests have been carried out. Thus, on the basis of these tests, the mean computation time is equal to 147-seconds for the detection of only one frequency signature, using the original Root-MUSIC method [1]. However, with the proposed method the estimated time is 0.85 seconds. Note that we obtained these results by considering a signal of 10000 samples and using a PC equipped with a dual-core processor of 2 GHZ and 3 GB of RAM.

Experimental Results

Description of Test Bench

The motor used in these practical tests is a three-phase squirrel cage motor, with parameters (see Appendix). This motor is coupled to a direct current generator connected to a resistive load to simulate a variable mechanical load. The Test bench used is illustrated in Fig.5.

Three Hall effect current sensors (Fluke i30s) are used to measure the three stator currents. All these electrical signals are digitized at the same time using NI USB-6229 type acquisition card with 08 inputs.

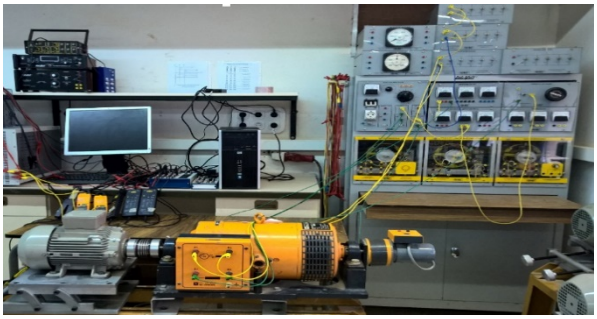

Fig.5. Photo of experimental test bench

The motor speed is measured using a tachometer (LUTRON DT-2236). The measurement chain is managed by a computer, which also allows the processing of acquired signals.

To show the effectiveness of the proposed window, different operating modes are tested with:

- A healthy rotor.
- A rotor with one broken bar.
- A rotor with two adjacent broken bars, in order to follow the severity of the fault.

Because of the random nature of the measured signals, several acquisitions were made for each operating mode to have a reliable analysis. All acquisitions are carried out in the steady state with an acquisition time of 11 seconds and a sampling frequency of 3 kHz. Under these conditions, the frequency resolution obtained is 0.09 Hz. Finally, broken bars are created artificially by drilling 1 mm holes on the cage rotor bars, as shown in Fig. 6.

According to the theoretical study, the frequency signatures of the rotor faults corresponding to the faulty operating modes are likely to appear around the fundamental frequency in the spectrum of the stator current. Knowing that, the induction motor slip never exceeds the value of 7 %. For this reason and for a better legibility of the spectrum, the spectral analysis can be carried out only on the frequency band [40Hz - 60 Hz].

Note that in this paper, the comparison between the proposed window and the rectangular window is justified because this technique is widely used in industry.

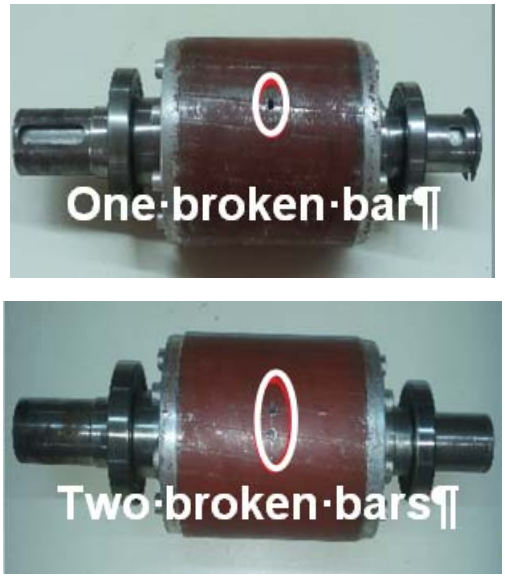

Fig. 6. Rotor faults -one and two adjacent broken bars

A Healthy Rotor

For operation with a healthy rotor and a nominal load, the measured rotor speed is 1431 rpm, which gives a slip of 4.6 %. For this slip value and according to equation (1), the theoretical frequency signatures of an eventual rotor fault, must appear around the fundamental at frequencies 45.4 Hz and 54.6 Hz. The spectrum of the stator current using the rectangular window is illustrated in Fig. 7.

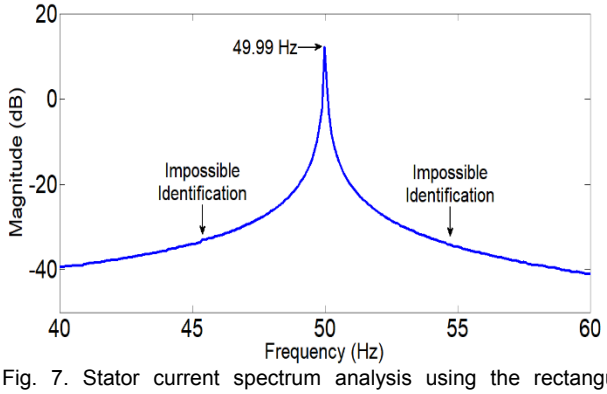

Fig. 7. Stator current spectrum analysis using the rectangular window. - Healthy Operation Mode –

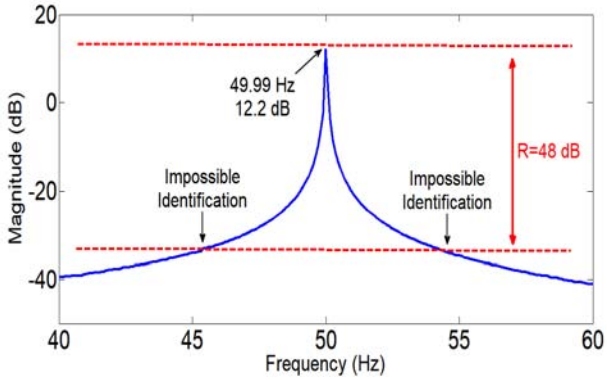

Fig. 8. Determination of Ratio *R* - Healthy Operation Mode-

From this figure, we notice that no signature appears around the fundamental with the use of the rectangular window, which seems logical for a rotor considered as healthy. To confirm this result by the proposed window, it is necessary to know the ratio *R* to determine the parameter *Z*.

The ratio *R* does not depend on the broken bars number or the rotor fault severity, but it depends on the fault frequency signature location, in other words, on the motor speed. For this reason, the motor speed must be correctly measured for a better estimation of *R*.

In these conditions, two indicative lines are drawing. The first upper straight line goes through the maximum of the fundamental. The second straight line goes through the possible location of the frequency signatures of the rotor fault, at 45.4 Hz and 54.6 Hz, as shown in Fig. 8.

According to this figure, *R* is equal to 48 dB, which gives, using equation (11) a value of 0.7 for the parameter *Z*

The stator current spectrum using the proposed window with *Z* equal to 0.7 and *D* equal to -0.5, is illustrated by the following figure.

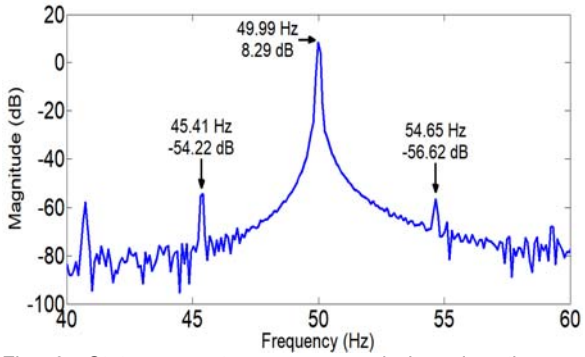

Fig. 9. Stator current spectrum analysis using the proposed window- Healthy Operation Mode-

The application of this new window shows the rise of two harmonics at 45.41 Hz and 54.65 Hz. The location of these frequencies corresponds to the theoretical ones for the obtained slip (4.6 %). The slight difference between the positions of the real frequencies and those of the theoretical frequencies is explained by the error in measuring the rotor speed.

The use of the proposed window made it possible to reveal these frequencies, which are certainly due to scratches on the rotor caused by the intensive use of the motor during the various tests. However, these frequencies cannot be considered as signatures of a faulty rotor.

Indeed, B. Xu [18] shows that when the magnitudes of these harmonics are less than -50 dB, the rotor is considered as healthy. In our example, Amplitude of these harmonics are respectively -54.22 dB and -56.62 dB. This very interesting result was not obtained with the rectangular window, hence the interest of the proposed window.

Finally, it should be noted that these results would be considered as a reference for all of the following operating modes.

A Rotor with one Broken Bar

For this operating mode, the rotor contains one broken bar and rotates with a rotor speed of 1455 rpm, which gives a slip of 3 %. For such a slip, the theoretical frequency signatures of the rotor fault must appear at frequencies 47 Hz and 53 Hz according to equation (1). The PSD estimation of the stator current with one broken bar using the rectangular window is illustrated in Fig.10.

From this figure, we notice the appearance of a very low amplitude signatures around the fundamental, difficult to identify which does not allow us to tell if the used rotor is faulty.

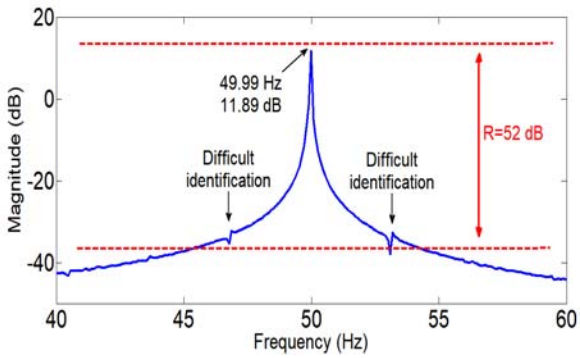

Fig. 10. Stator current spectrum analysis using the rectangular window- One Broken Bar –

To apply the proposed method, it is essential to know the ratio *R*. For this, the first straight line always goes through the maximum amplitude of the fundamental frequency. The second straight line goes through the location of the theoretical frequency signatures of the fault (47 Hz and 53 Hz) as illustrated in Fig. 10. The plot of both lines gives a *R* ratio of 52 dB. The variation of the value of *R* compared to the healthy case is due to the change of slip, which is in this case equal to 3%. For this value of *R* and using equation (11), the value of *Z* equal to 0.8.

The spectrum of the stator current using the proposed window with a value of *Z* equal to 0.8 and *D* equal to -0.5, is illustrated by Fig. 11.

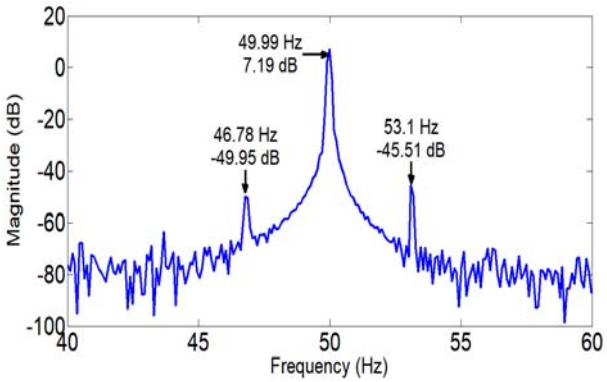

Fig. 11. Stator current spectrum analysis using the proposed window - One Broken Bar -

According to Fig. 11, the fault signatures are much more readable (46.78 Hz, 53.1 Hz) compared to the results obtained with the rectangular window (Fig. 10). In addition, the magnitudes of these signatures (-49.95 dB, -45.51 dB) are greater than those of the healthy case (see Fig. 9), which explains why the fault is more pronounced.

A Rotor with Two Broken Bars

In this last operating mode, the stator current is analyzed when the rotor contains two adjacent broken bars.

The measured rotor speed in this test is 1434 rpm, which gives a slip of 4.4 %. In this case, the theoretical frequency signatures of the fault must appear around the fundamental at frequencies 45.6 Hz and 54.4 Hz. Fig. 12, presents the PSD estimation of the stator current using the rectangular window.

According to this figure, the fault frequency signatures are more readable at (45.59 Hz / -31.96 dB) and (54.38 Hz / -33.44 dB) compared to the previous case, which shows the increase of the fault severity.

In the same way as the previous operating modes, it is essential to know the ratio *R* in order to be able to properly calculate the value of the parameter *Z* of the proposed

window. The plot of both lines (see Fig. 12), gives *R* of 45 dB, which gives a value of 0.6 for the parameter *Z*.

For this value of *Z* and for a *D* always equal to -0.5, the stator current spectrum obtained using the proposed window is illustrated by Fig. 13.

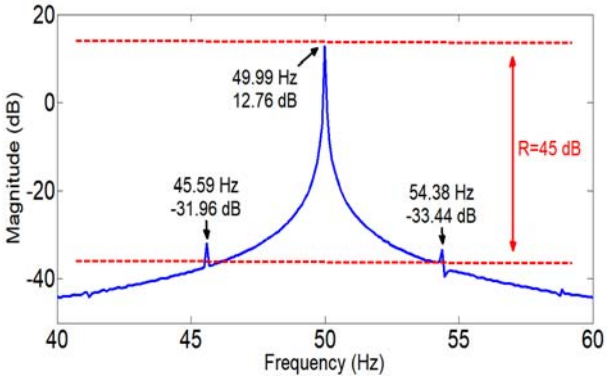

Fig. 12. Stator current spectrum analysis using the rectangular window- Two Broken Bars –

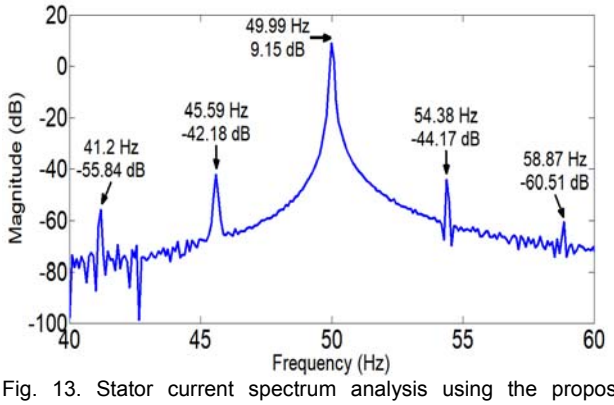

Fig. 13. Stator current spectrum analysis using the proposed window- Two Broken Bars -

This figure shows that, using the proposed window with the obtained *Z*, allows the detection of the first fault harmonics at 45.59 Hz and 54.38 Hz, but with an increase in their magnitudes (-42.18 dB, - 44.17 dB) compared to the rotor with a single broken bar (see Fig. 11). In addition, other signatures appeared at frequencies 41.2 Hz and 58.87 Hz with the respective magnitudes of -55.84 dB and -60.51 dB. These signatures characterize the multiple frequencies of the rotor fault; see equation (1) for *k* equals to 2. The appearance of these two harmonics shows that the severity of the fault is more important.

From the obtained results, it is clear to note that the window proposed is an indicator of the severity of the rotor fault. Indeed, the use of this new window enables the monitoring of the number of broken rotor bars by a simple monitoring of the fault signature evolution. The following table summarizes these findings.

Table 2. Amplitude variation of the first harmonic of the lower sideband

Rotor state	Healthy Rotor	One Broken Rotor Bar	Two Broken Rotor Bars
Rectangular window	Impossible identification	Difficult identification	-31.96 dB
Proposed window	- 54.22 dB	- 49.95 dB	- 42.18 dB

Conclusion

In this paper, a new window function is proposed with an adequate calculation of its shape parameters *D* and *Z*, in order to improve the diagnosis of an incipient rotor fault of induction motors. To this end, a mathematical relationship allowing the calculation of the parameter *Z* is developed from the data of the acquired signal spectrum of stator current, to ensure a better compromise between the width of the main lobe and the maximum amplitude of the side lobes. In the light of the experimental results, the efficiency of the proposed window and its power to identify the frequency signatures of the incipient rotor faults are clearly demonstrated, while preserving the main advantages of the conventional PSD estimation method in the term of simplicity of programming and speed of execution. In addition, the obtained results showed the performance of the use of the proposed window with the parameters calculated in the monitoring of the rotor fault severity investigated in this paper.

Appendix

Rated power	3 KW
Supply frequency	50 Hz
Rated voltage	380 V
Rated current	7 A
Rated speed	1410 rpm
Number of rotor bars	28
Number of pole pairs	2

Acknowledgments

The authors would like to thank all the members of the Laboratory of Development of Electric Drives of the University of Sciences and Technology of Oran, Mohamed Boudiaf, USTO-MB, ALGERIA, for the help they brought to the experimental validation of this work.

***Authors**:*

Mr. Mohamed Boudiaf KOURA, PhD student, Laboratory of Electric Drives Development, Diagnosis Group, Department of Electrical Engineering, University of Sciences and Technology of Oran, Oran, Algeria, E-mail: mohamedboudiaf.koura@univ-usto.dz.

prof. Ahmed Hamida BOUDINAR, Laboratory of Electric Drives Development, Diagnosis Group, Department of Electrical Engineering, University of Sciences and Technology of Oran, Oran, Algeria, E-mail: ahmed.boudinar@univ-usto.dz.

prof. Azeddine BENDIABDELLAH, Laboratory of Electric Drives Development, Diagnosis Group, Department of Electrical Engineering, University of Sciences and Technology of Oran, Oran, Algeria, E-mail: bendiazz@yahoo.fr

dr. Ameur Fethi AIMER, Laboratory of Electric Drives Development, Diagnosis Group, Department of Electrical Engineering, University of Sciences and Technology of Oran, Oran, Algeria, E-mail: fethi.aimer@yahoo.fr

Mr. Zakaria GHERABI, PhD student, Laboratory of Electric Drives Development, Diagnosis Group, Department of Electrical Engineering, University of Sciences and Technology of Oran, Oran, Algeria, E-mail: zakariagherabi@gmail.com

REFERENCES

[1] A. H. Boudinar, N. Benouzza, A. Bendiabdellah, et M. Khodja," Induction Motor Bearing Fault Analysis Using a Root-MUSIC Method," *IEEE Transactions on Industry Applications*. 52 (2016), No. 5, 3851–3860.

[2] A. H. Bonnett et C. Yung," Increased Efficiency Versus Increased Reliability," *IEEE Industry Applications Magazine*. 14 (2008), No. 1, 29–36.

[3] J. A. Antonino-Daviu, J. Pons-Llinares, et S. B. Lee," Advanced Rotor Fault Diagnosis for Medium-Voltage Induction Motors Via Continuous Transforms," *IEEE Transactions on Industry Applications*. 52 (2016), No. 5, 4503–4509.

[4] D. G. Jerkan, D. D. Reljić, et D. P. Marčetić," Broken Rotor Bar Fault Detection of IM Based on the Counter-Current Braking Method," *IEEE Transactions on Energy Conversion*. 32 (2017), No. 4, 1356–1366.

[5] H. Henao et al," Trends in Fault Diagnosis for Electrical Machines: A Review of Diagnostic Techniques," *IEEE Ind. Electron*. 8 (2014), No.2, 31–42.

[6] M. Iorgulescu et R. Beloiu," Faults diagnosis for electrical machines based on analysis of motor current" *in International Conference on Optimization of Electrical and Electronic Equipment (OPTIM)*, Bran, Romania. (2014), 291–297.

[7] P. A. Panagiotou, I. Arvanitakis, N. Lophitis, J. Antonino-Daviu, et K. N. Gyftakis," A New Approach for Broken Rotor Bar Detection in Induction Motors Using Frequency Extraction in Stray Flux Signals," *IEEE Transactions on Industry Applications*. 55 (2019), No. 4, 3501–3511.
[8] M. Z. Ali, M. N. S. K. Shabbir, X. Liang, Y. Zhang, et T. Hu," Machine Learning-Based Fault Diagnosis for Single- and Multi-Faults in Induction Motors Using Measured Stator Currents and Vibration Signals," *IEEE Transactions on Industry Applications*. 55 (2019), No. 3, 2378–2391.
[9] Praveen Kumar N et Isha T B," Electromagnetic field analysis of 3-Phase induction motor drive under broken rotor bar fault condition using FEM," *IEEE International Conference on Power Electronics, Drives and Energy Systems (PEDES)*. (2016), 1–6.
[10] M. Aberkane, N. Benouzza, A. Bendiabdellah, et A. H. Boudinar," Discrimination between Supply Unbalance and Stator Short-Circuit of an Induction Motor Using Neural Network," *International Review of Automatic Control (IREACO)*. 10 (2017), No. 5, 451–460.
[11] I. Ouachtouk, S. E. Hani, S. Guedira, K. Dahi, et H. Mediouni," Broken rotor bar fault detection based on stator current envelopes analysis in squirrel cage induction machine," *in IEEE International Electric Machines and Drives Conference (IEMDC)*, Miami, FL, USA. (2017) 1–6.
[12] M.-E.-A. Khodja, A. H. Boudinar, et A. Bendiabdellah," Effect of Kaiser Window Shape Parameter for the Enhancement of Rotor Faults Diagnosis,". *International Review of Automatic Control (IREACO)*. 10 (2017), No. 6, 461-467.
[13] M. Sahraoui, A. J. M. Cardoso, et A. Ghoggal," The Use of a Modified Prony Method to Track the Broken Rotor Bar Characteristic Frequencies and Amplitudes in Three-Phase Induction Motors," *IEEE Trans. on Ind. Applicat*. 51 (2015), No. 3, 2136–2147.
[14] J. Grande-Barreto, C. Morales-Perez, J. Rangel-Magdaleno, et H. Peregrina-Barreto," Half-broken bar detection using MCSA and statistical analysis," *in IEEE International Autumn Meeting on Power, Electronics and Computing (ROPEC)*, Mexico. (2017), 1–5.
[15] A. Bellini et al," On-field experience with online diagnosis of large induction motors cage failures using MCSA," *IEEE Transactions on Industry Applications*. 38 (2002), No. 4, 1045–1053.
[16] J. Zhuzhi, Z. Hongyu, L. Xuyang, et S. Hang," Incipient Broken Rotor Bar Fault Diagnosis Based on Extended Prony Spectral Analysis Technique," *in 37th Chinese Control Conference (CCC), Wuhan, China*. (2018), 5705–5710.
[17] Y. Kim, Y. Youn, D. Hwang, J. Sun, et D. Kang," High-Resolution Parameter Estimation Method to Identify Broken Rotor Bar Faults in Induction Motors," *IEEE Transactions on Industrial Electronics*. 60 (2013), No.9, 4103–4117.
[18] B. Xu, L. Sun, L. Xu, et G. Xu," Improvement of the Hilbert Method via ESPRIT for Detecting Rotor Fault in Induction Motors at Low Slip," *IEEE Transactions on Energy Conversion*. 28 (2013), No. 1, 225–233.
[19] M. B. Koura, A. H. Boudinar, et A. F. Aimer," Improved Diagnosis of Induction Motor's Rotor Faults using the Papoulis Window," *in 2019 International Aegean Conference on Electrical Machines and Power Electronics (ACEMP) 2019 International Conference on Optimization of Electrical and Electronic Equipment (OPTIM)*. (2019), 216–220.
[20] H. Wen, Z. Teng, Y. Wang, et Y. Yang," Optimized Trapezoid Convolution Windows for Harmonic Analysis," *IEEE Transactions on Instrumentation and Measurement*. 62 (2013), No. 9, 2609–2612.
[21] M. Mottaghi-Kashtiban et M. G. Shayesteh," New efficient window function, replacement for the Hamming window," *IET Signal Processing*. 5 (2017), No. 5, 499-505.
[22] S. Williamson et A. C. Smith," Steady-state analysis of 3-phase cage motors with rotor-bar and end-ring faults," *IEE Proceedings B - Electric Power Applications*. 129 (2017), No.3, 93-100.
[23] G. B. Kliman, R. A. Koegl, J. Stein, R. D. Endicott, et M. W. Madden," Noninvasive detection of broken rotor bars in operating induction motors," *IEEE Transactions on Energy Conversion*. 3 (1988), No. 4, 873–879.
[24] F. Filippetti, G. Franceschini, C. Tassoni, et P. Vas," AI techniques in induction machines diagnosis including the speed ripple effect," *IEEE Transactions on Industry Applications*. 34 (2017), No. 1, 98–108.
[25] H. Henao, H. Razik, et G.-A. Capolino," Analytical Approach of the Stator Current Frequency Harmonics Computation for Detection of Induction Machine Rotor Faults," *IEEE Trans. on Ind. Applicat*. 41 (2005), No. 3, 801–807.
[26] G. B. Kliman et J. Stein," Methods of Motor Current Signature Analysis," *Electric Machines & Power Systems*. 20 (1992), No. 5, 463–474.
[27] A. F. Aimer, A. H. Boudinar, N. Benouzza, et A. Bendiabdellah," Simulation and experimental study of induction motor broken rotor bars fault diagnosis using stator current spectrogram," *in 3rd International Conference on Control, Engineering Information Technology (CEIT)*, Tlemcen, Algeria. (2015), 1–7.
[28] A. Papoulis," Minimum-bias windows for high-resolution spectral estimates," *IEEE Transactions on Information Theory*. 19 (1973), No. 1, 9–12.
[29] F. J. Harris," On the use of windows for harmonic analysis with the discrete Fourier transform," *Proceedings of the IEEE*. 66 (1978), No. 1, 51–83.
[30] K. M. M. Prabhu, Window Functions and Their Applications in Signal Processing. CRC Press, 2018.